

# Probing invisible dark photon models via atmospheric collisions

Mingxuan Du,<sup>1</sup> Rundong Fang,<sup>2</sup> Zuwei Liu,<sup>2</sup> Wenxi Lu,<sup>2</sup> and Zicheng Ye<sup>2</sup>

<sup>1</sup>*Center for High Energy Physics, Peking University, Beijing 100871, China*

<sup>2</sup>*Department of Physics, Nanjing University, Nanjing 210093, China*

Atmospheric collisions can copiously produce dark sector particles in the invisible dark photon model, leading to detectable signals in underground neutrino detectors. We consider the dark photon model with the mass mixing mechanism and use the Super-K detector to detect the electron recoil events caused by the atmospherically produced dark sector particles within the model. We find that the combined data from four Super-K runs yield new leading constraints for the invisible dark photon in the mass range of  $\sim (0.5 - 1.4)$  GeV, surpassing the constraints from NA64, BaBar, and searches for millicharged particles.

## I. INTRODUCTION

The nature of dark matter remains elusive, in spite of decades of dedicated efforts [1, 2]. In recent years there has been increased interest in models where dark matter resides in a dark sector and interacts with the standard model sector through the interactions of a dark photon [3–6]. Dark photon can arise in models where a new abelian gauge boson in the dark sector mixes with the hypercharge boson in the standard model via either the kinetic mixing mechanism [7, 8] or the mass mixing mechanism [9–13].

Accelerator experiments are optimal environments for probing dark photons with mass above MeV [6]. For dark photons with a substantial decay width into standard model particles, one of the key detection channels involves identifying distinct peaks in the invariant mass distribution of the decay products. However, it is more challenging at accelerator experiments to detect the dark photon that decays predominantly into the dark matter final state. We refer to this kind of dark photon as the “invisible dark photon”. At the sub-GeV mass range, the current best constraints on the invisible dark photon are from the electron beam-dump experiment NA64 [14, 15] and the electron collider BaBar [16]. The detection channels are the missing energy signature at NA64 [14, 15] and the mono-photon signature at BaBar [16], respectively.

In this study we consider cosmic ray interactions with the Earth’s atmosphere as the source of dark matter production within the invisible dark photon model. Recent studies have shown that the atmospheric collisions of cosmic rays can lead to a copious generation of sub-GeV dark matter particles, consequently presenting a novel avenue for probing the dark sector [17–22]. In this paper we consider the dark photon model with a mass mixing term and use the neutrino experiment Super-K to detect dark matter originating from atmospheric collisions. We find that the combined data from four Super-K runs yield new leading constraints on the invisible dark photon in the mass range of  $\sim (0.5 - 1.4)$  GeV.

## II. THE MODEL

We consider the dark photon model that has a mass mixing term:

$$\mathcal{L} = \mathcal{L}_{\text{SM}} - \frac{1}{4} \tilde{F}'_{\mu\nu} \tilde{F}'^{\mu\nu} + \frac{\tilde{m}_{A'}^2}{2} (\tilde{A}'_\mu + \epsilon \tilde{A}_\mu)^2 + \bar{\chi} (i\gamma^\mu \partial_\mu - m_\chi + g_d \gamma^\mu \tilde{A}'_\mu) \chi \quad (1)$$

where  $\tilde{A}$  is the gauge photon,  $\tilde{A}'$  is the new  $U(1)_d$  gauge boson in the dark sector with  $\tilde{F}'^{\mu\nu}$  being the field strength,  $\chi$  is the Dirac fermion in the dark sector charged under the  $U(1)_d$  gauge,  $m_\chi$  is the mass of  $\chi$ ,  $\tilde{m}_{A'}$  is the mass of the new gauge boson, and  $\epsilon$  is the dimensionless mass mixing parameter. The mass terms can be naturally generated in the Stueckelberg mechanism; see e.g., Ref. [12] for mass mixing terms with the hypercharge boson.

The mass matrix can be diagonalized by the following transformation [12]

$$\begin{bmatrix} \tilde{A}_\mu \\ \tilde{A}'_\mu \end{bmatrix} = \kappa \begin{bmatrix} 1 & \epsilon \\ -\epsilon & 1 \end{bmatrix} \begin{bmatrix} A_\mu \\ A'_\mu \end{bmatrix}, \quad (2)$$

where  $\kappa \equiv 1/\sqrt{1 + \epsilon^2}$ . This leads to a massless state  $A_\mu$ , which is identified as the photon, and a massive eigenstate  $A'_\mu$  with a mass of  $m_{A'} = \tilde{m}_{A'}/\kappa$ , which is the dark photon. In the parameter space of interest in this analysis, one has  $\kappa \simeq 1$ . The interaction Lagrangian in terms of the mass eigenstates is

$$\mathcal{L}_{\text{int}} = \kappa (\epsilon J_\mu^{\text{EM}} + J'_\mu) A'^\mu + \kappa (J_\mu^{\text{EM}} - \epsilon J'_\mu) A^\mu, \quad (3)$$

where  $J_\mu^{\text{EM}}$  and  $J'_\mu = g_d \bar{\chi} \gamma_\mu \chi$  are the currents in the standard model sector and the dark sector, respectively. The coupling between  $\chi$  and  $A_\mu$  is suppressed by the small parameter  $\epsilon$ , leading to a millicharge of  $Q_\chi = g_d \epsilon \kappa / e$  for  $\chi$ , where  $e$  is the QED coupling. Note that in this model, the dark sector fermion  $\chi$  interacts with both the dark photon and the photon. This is different from the model with a kinetic mixing term, i.e.,  $(\epsilon/2) \tilde{F}'_{\mu\nu} \tilde{F}^{\mu\nu}$ , where a massive  $A'$  and a millicharged  $\chi$  cannot appear simultaneously [12]; this then leads to a weaker limit in the kinetic mixing case due to the absence of the photon-mediated processes, as shown in Fig. (2).

In this paper we consider the following parameters:  $\epsilon \ll 1$ ,  $\alpha_d \equiv g_d^2/4\pi = 0.1$ , and  $m_{A'} = 3m_\chi$ ; in this case, the dark photon decays predominantly into  $\chi$  and its decay width into the standard model particles is negligible. Thus, we use the invisible decay width  $\Gamma(A' \rightarrow \chi\bar{\chi})$  to approximate the total decay width:

$$\Gamma_{A'} = \frac{\alpha_d}{3} m_{A'} \left( 1 + \frac{2m_\chi^2}{m_{A'}^2} \right) \sqrt{1 - \frac{4m_\chi^2}{m_{A'}^2}}. \quad (4)$$

### III. ATMOSPHERIC FLUX

In this section we compute the flux of  $\chi$  generated by cosmic ray collisions with the atmosphere, by using the one-dimension approximation [23]. The flux of  $\chi$  on the Earth surface is isotropic in the one-dimension approximation and is given by [23] [22]

$$\frac{d^2\Phi_\chi^s}{dE_\chi^s d\Omega_\chi^s} = \iint dh dE_p \frac{d^2\Phi_p(h)}{dE_p d\Omega_p} n_T(h) \sigma_{pT} \sum_i \frac{dN_\chi^i}{dE_\chi^s}, \quad (5)$$

where  $h$  is the altitude,  $E_\chi^s$  ( $E_p$ ) is the energy of  $\chi$  (proton),  $\Omega_\chi^s$  ( $\Omega_p$ ) is the solid angle of  $\chi$  (proton),  $\Phi_\chi^s$  is the flux of  $\chi$  at the surface of Earth,  $\Phi_p(h)$  is the cosmic ray proton flux at altitude  $h$ ,  $n_T(h)$  is the number density of the target nucleus  $T$  in the atmosphere at altitude  $h$ ,  $\sigma_{pT}$  is the in-elastic proton-air cross section, and  $dN_\chi^i/dE_\chi^s$  is the energy spectrum of  $\chi$  per proton-air collision in the production channel denoted by the superscript  $i$ . We use CRMC [24, 25] to compute  $\sigma_{pT}$  for nitrogen and oxygen; because of the weak energy dependence in the region of interest, we use a constant cross section  $\sigma_{pT} \simeq 253$  (281) mb for nitrogen (oxygen). We use the NRLMSISE-00 atmosphere model [26] for the air density  $n_T(h)$ . To compute the cosmic ray proton flux at altitude  $h$ , we solve the cascade equation [23]

$$\frac{d}{dh} \frac{d^2\Phi_p(h)}{dE_p d\Omega_p} = \sigma_{pT} n_T(h) \frac{d^2\Phi_p(h)}{dE_p d\Omega_p}, \quad (6)$$

with the power law distribution for cosmic ray protons at  $h_{\max} = 65$  km [27]

$$\frac{d^2\Phi_p(h_{\max})}{dE_p d\Omega_p} = \frac{0.74 \times 1.8 \times 10^4}{\text{m}^2 \text{sr GeV}} \left( \frac{E_p}{\text{GeV}} \right)^{-2.7}. \quad (7)$$

There are two production channels of  $\chi$  in atmospheric collisions: production of  $\chi$  in meson decays [18, 20, 21], and production of  $\chi$  in the proton bremsstrahlung process [22]. As recently pointed out by Ref. [22], the proton bremsstrahlung process is the dominant process of producing millicharged particles in the sub-GeV mass range. For example, the millicharged particle flux arising from meson decays is less than 0.5% of that from the proton bremsstrahlung process for mass  $\sim 0.2$  GeV [22]. Since the dark sector fermion  $\chi$  in the model considered here is similar to millicharged particles in the minimal

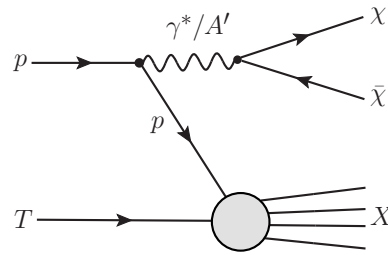


Figure 1. Production of  $\chi$  in the proton bremsstrahlung process in collisions between the cosmic proton  $p$  and the nucleus  $T$  in the atmosphere.

model considered in Ref. [22], we only consider the proton bremsstrahlung process as the production channel.

The Feynman diagrams of the proton bremsstrahlung process for the dark photon model considered in this paper are shown in Fig. (1); the mediator to produce a pair of  $\chi$ 's can be either a photon or a dark photon. Ref. [22] computed the production of millicharged particles in the proton bremsstrahlung process where only the virtual photon mediator was taken into account. Here we further include the contribution from the dark photon mediator. Thus, the energy spectrum of  $\chi$  in the proton bremsstrahlung process is given by

$$\frac{dN_\chi}{dE_\chi} = \frac{\epsilon^2 g_d^2}{6\pi^2} \int \frac{dk^2}{k^2} \frac{(2k^2 - m_{A'}^2)^2 + m_{A'}^2 \Gamma_{A'}^2}{(k^2 - m_{A'}^2)^2 + m_{A'}^2 \Gamma_{A'}^2} \sqrt{1 - 4x} \\ \times (1 + 2x) \int \frac{dE_k}{\sigma_{pT}} \frac{d\sigma_{PB}}{dE_k} \frac{\Theta(E_\chi - E_-) \Theta(E_+ - E_\chi)}{E_+ - E_-}, \quad (8)$$

where  $E_\chi$  is the energy of  $\chi$  in the lab frame,  $k^\mu = (E_k, \vec{k})$  is the momentum of the virtual photon  $\gamma^*$  or the dark photon  $A'$ ,  $\Gamma_{A'}$  is the total decay width of the dark photon,  $x = m_\chi^2/k^2$ ,  $d\sigma_{PB}/dE_k$  is the differential cross section for the inclusive process of  $pN \rightarrow \gamma^* X$ ,  $E_\pm \equiv \gamma(E_\chi \pm \beta p_\chi^r)$  denote the maximal and minimum values of  $E_\chi$  with  $\gamma = (1 - \beta^2)^{-1/2} = E_k/\sqrt{k^2}$ , and  $E_\chi^r$  ( $p_\chi^r$ ) is the energy (magnitude of momentum) of  $\chi$  in the rest frame of  $\gamma^*/A'$ . The expression of  $d\sigma_{PB}/dE_k$  can be found in Ref. [22].

### IV. EARTH ATTENUATION

In order to precisely obtain the flux of  $\chi$  at underground neutrino detectors, it is necessary to take into account the Earth's attenuation effect. Charged particles lose energy through ionization and radiative processes as they traverse a medium [28]; for low-energy charged particles, ionization is usually the dominant process. Since the mass of  $\chi$  of interest in this analysis falls within the range of  $\sim (0.1 - 1)$  GeV, we follow Ref. [21] and use Earth's attenuation effects on muons as a reference to account for the energy loss of  $\chi$ .

Thus, the energy loss of  $\chi$  along the trajectory tra-

versed in Earth can be computed as follows [21, 29]

$$-\frac{dE}{dX} = Q_\chi^2(a + bE), \quad (9)$$

where  $X$  is the slant depth traversed, and  $a$  ( $b$ ) is the parameter to describe energy loss due to ionization (radiation in scatterings with nuclei). In our analysis we adopt the parameters for muons in the standard rock:  $a = 0.233$  GeV/mwe and  $b = 4.64 \times 10^{-4}$  mwe $^{-1}$  where 1 mwe = 100 g/cm $^2$  [30]. The slant depth  $X$  for the Super-K detector is given by  $X = \rho L$  where  $\rho = 2.6$  g/cm $^3$  is the mass density of the standard rock, and  $L$  is the distance travelled in the rock. We compute  $L$  via

$$L = \sqrt{(2R_e^2 - 2R_e d)(1 - \cos(\theta - \theta_s)) + d^2}, \quad (10)$$

where  $R_e$  is the radius of Earth,  $d = 1$  km is the depth of the Super-K detector [31],  $\theta_s$  is the zenith angle of the MCP at the Earth surface, and  $\theta$  is the zenith angle of the Super-K detector. By solving Eq. (9), the MCP flux at the Super-K detector is given by

$$\frac{d^2\Phi_\chi^D(X)}{dE_\chi^D d\Omega^D} = \exp(Q_\chi^2 bX) \frac{d^2\Phi_\chi^s}{dE_\chi^s d\Omega^s}, \quad (11)$$

where the superscripts  $D$  and  $s$  denote the physical quantities at the detector and at the Earth surface, respectively, and  $E_\chi^s = (E_\chi + a/b) \exp(Q_\chi^2 bX) - a/b$ .

## V. SIGNALS AT SUPER-K

In our analysis we consider the Super-K detector, a large water-Cherenkov detector with a fiducial volume of 22.5 kton of water [31]. For the invisible dark photon model, the dominant signals in Super-K come from the elastic scattering between the dark sector fermion  $\chi$  and the target electron, which can be mediated by either the photon or the dark photon. Thus, the  $\chi - e$  scattering cross section is given by

$$\begin{aligned} \frac{d\sigma}{dE_r} = & \pi\alpha\alpha_d\epsilon^2 \frac{E_r + 2E_\chi^2/E_r - 2E_\chi - m_e - m_\chi^2/m_e}{(E_\chi^2 - m_\chi^2)m_e E_r} \\ & \times \left( \frac{4m_e E_r + m_{A'}^2}{2m_e E_r + m_{A'}^2} \right)^2, \end{aligned} \quad (12)$$

where  $E_\chi$  is the energy of  $\chi$ ,  $E_r$  is the recoil energy of the electron, and  $m_e$  is the electron mass.

In our analysis we use electron recoil data from four Super-K runs with a total exposure of 176 kton-year [32, 33]. The electron recoil data in Super-K are selected by the Cherenkov angle in the range of 38-50 degrees, since relativistic charged particles (such as electrons in the energy range of interest) have a Cherenkov angle of 42 degrees, whereas heavier particles have a smaller Cherenkov angle [32, 33]. The Super-K I-III data in the

electron recoil energy range of 16-88 MeV are binned into 18 bins with a bin width of 4 MeV for each data bin [32]; the Super-K IV data in the electron recoil energy range of 16-78 MeV are binned into 31 bins with a bin width of 2 MeV for each data bin [33]. We compute the signal events  $S_i$  in each data bin via

$$S_i = 2\pi n_e \mathcal{E} \int dE_r f(E_r) \int dE_\chi dz \frac{d^2\Phi_\chi^D}{dE_\chi dz} \frac{d\sigma}{dE_r}, \quad (13)$$

where  $z \equiv \cos\theta$ ,  $n_e$  is the number of electrons per ton of water,  $\mathcal{E}$  is the exposure, and  $f(E_r)$  is the detector efficiency. In our analysis we adopt the efficiency curve in Fig. (10) of Ref. [32].

Because of Earth's attenuation, in the parameter space of interest, the  $\chi$  flux with  $\theta > 90^\circ$  are significantly suppressed compared to that with  $\theta < 90^\circ$ , where  $\theta$  is the zenith angle. However, the background events are not suppressed in the  $\theta > 90^\circ$  region. Note that, in the parameter space of interest, the recoiled electron has almost the same direction as the incident  $\chi$ . Thus, to suppress background events, we take the electron recoil data in the range of  $\theta < 90^\circ$  as the signal region.

In the low energy region of the electron recoil data (16 MeV  $\lesssim E_r \lesssim 55$  MeV), the dominant backgrounds are due to electrons from decays of very low-energy muons that originate in the charged-current (CC) process of muon-neutrinos [32, 33]. These low-energy muon decays give rise to an isotropic electrons background. In the high energy region (55 MeV  $\lesssim E_r \lesssim 88$  MeV), the dominant backgrounds come from the CC process of the electron-neutrinos [32, 33]. The angular distribution of the electron-neutrino flux is not isotropic: it has a peak near  $\theta = 90^\circ$  and exhibits an upward-downward asymmetry with more neutrinos from the region of  $\theta > 90^\circ$  compared to the region of  $\theta < 90^\circ$  [34]. For example, the electron-neutrino flux with energy of 0.32 GeV in the region of  $\theta < 60^\circ$  is about 18% of the flux from all angles [34]. However, the  $\chi$  flux in the region of  $\theta < 60^\circ$  is about 50% of the signal flux from all angles. Thus, we multiply a factor of half to the data events in Ref. [32, 33] to obtain the data events in the signal region,  $\theta < 90^\circ$ . We note that one could take advantage of the different angular distributions of the signal and background events in the high energy region to further improve the constraints.

## VI. RESULTS

To set upper bounds on the dark photon model, we take a background-agnostic approach [21] [35] such that the likelihood function are constructed only by the data bins in which the predicted signal events (without background) are more than the observed data events. For each data bin, we construct the likelihood function via

$$\mathcal{L}_i = \begin{cases} P(D_i|S_i) & D_i \leq S_i \\ 1 & D_i > S_i \end{cases}, \quad (14)$$

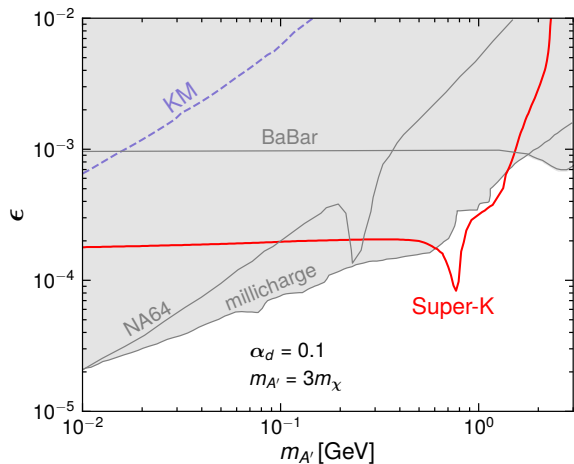


Figure 2. Super-K constraints (90% CL) on the mass mixing parameter  $\epsilon$  in the invisible dark photon model (red solid). Super-K constraints on the kinetic mixing dark photon model are also shown (blue dashed). Existing constraints are shown as gray shaded regions: constraints on the invisible dark photon model from NA64 [15] and BaBar [16], and constraints on the millicharge of the dark fermion. For the dark photon model, we fix  $m_{A'} = 3m_\chi$  and  $\alpha_d = 0.1$ .

where  $P(D_i|S_i)$  is the Poisson distribution:

$$P(D_i|S_i) = \frac{(S_i)^{D_i}}{D_i!} \exp(-S_i), \quad (15)$$

with  $D_i$  and  $S_i$  being the data events and expected signal events in the  $i$ -th bin, respectively. The total likelihood is given by  $\mathcal{L} = \prod_i \mathcal{L}_i$ , and the test statistics is given by

$$\mathcal{TS} = -2 \log \left[ \frac{\mathcal{L}(m_\chi, \epsilon)}{\mathcal{L}(m_\chi, \epsilon = 0)} \right]. \quad (16)$$

We use  $\mathcal{TS} < 4.6$  to set the 90% confidence level upper bound on the dark photon model.

Fig. (2) shows the Super-K 90% CL constraints on the mass mixing parameter  $\epsilon$  in the invisible dark photon model, where we use the data from four Super-K runs with a total exposure of 176 kton-year. For the invisible dark photon in the mass range of  $\sim (0.1 - 1.4)$  GeV (except the small region near  $\sim 0.2$  GeV), the Super-K constraints surpass the current best limits from NA64 [15] and BaBar [16].

Because in our dark photon model, the dark sector fermion  $\chi$  is millicharged, this model also receives constraints from searches of millicharged particles. Fig. (2) shows the currently best millicharge constraints in the parameter space of interest, including SLAC mQ [36], LSND [37], BEBC [38], and SENSEI [39]. As shown in Fig. (2), the Super-K limits analysed in this work is better than all other constraints for dark photon in the mass range of  $\sim (0.55 - 1.4)$  GeV.

The results shown in Fig. (2) are obtained with the power-law spectrum of cosmic protons given in Eq. (7).

However, low-energy protons are prevented by the geomagnetic field from scattering with the main distribution of the atmosphere at low altitude. Ref. [22] found that the results obtained with the power-law spectrum are consistent with the actual cosmic proton data, such as those from AMS-02 [40]. To estimate the effects of the geomagnetic field, we first equate the altitude of the AMS-02 experiment with the gyroradius of the proton at the Super-K to determine the cut-off energy on the cosmic proton, which is found to be  $\sim 5$  GeV. We then recompute the Super-K limits by excluding cosmic protons with  $E < 5$  GeV in Eq. (7), and find that the Super-K limits shown in Fig. (2) are unchanged in the dark photon mass range of  $\gtrsim 0.5$  GeV. The above statement holds even for a cut-off energy of 10 GeV. However, the geomagnetic field does have noticeable effects in the dark photon mass range of  $\lesssim 0.5$  GeV, resulting in somewhat weaker limits.

The stronger constraints in the vicinity of the dark photon mass of  $\sim 0.77$  GeV are primarily due to the time-like form factor of the various  $\rho/\omega$  vector mesons [22, 41–45], which are included in the computation of  $d\sigma_{\text{PB}}/dE_k$  in Eq. (8); see Ref. [22] for more details. This is because when the dark photon mass is close to the lowest  $\rho/\omega$  meson mass ( $\sim 0.77$  GeV), there is an enhancement on the signal from the Breit-Wigner distributions both of the dark photon and of the time-like form factor of  $\rho/\omega$ .

We note that the constraints on millicharged particles shown in Fig. (2) are analyzed in the minimal model where the effects of dark photon are neglected. The presence of a dark photon with mass comparable to the millicharged particle could potentially alter the signal significantly. We leave this to a future study.

## VII. CONCLUSIONS

In this paper we study the Super-K constraints on the invisible dark photon model with a mass mixing parameter. We use cosmic proton collisions with the Earth's atmosphere to copiously produce the dark sector fermion in the invisible dark photon model, which then leads to a detectable electron recoil signal in the Super-K detector. By carefully investigating the Earth's attenuation effects and the angular distributions of both the signal events and the background events, we find that the combined data from the four Super-K runs provide a new leading constraint on the invisible dark photon in the mass of  $\sim (0.55 - 1.4)$  GeV.

## ACKNOWLEDGMENTS

*Acknowledgments.* — We thank Li-Gang Xia and Yong-Heng Xu for discussions. The work is supported in part by the National Natural Science Foundation of China under Grant Nos. 12275128 and 12147103.



- [1] G. Bertone and D. Hooper, “History of dark matter,” *Rev. Mod. Phys.* **90** (2018) 045002 [[arXiv:1605.04909](#)].
- [2] A. Arbey and F. Mahmoudi, “Dark matter and the early Universe: a review,” *Prog. Part. Nucl. Phys.* **119** (2021) 103865 [[arXiv:2104.11488](#)].
- [3] J. Alexander *et al.*, “Dark Sectors 2016 Workshop: Community Report.” [arXiv:1608.08632](#).
- [4] M. Battaglieri *et al.*, “US Cosmic Visions: New Ideas in Dark Matter 2017: Community Report.” [arXiv:1707.04591](#).
- [5] J. Jaeckel and A. Ringwald, “The Low-Energy Frontier of Particle Physics,” *Ann. Rev. Nucl. Part. Sci.* **60** (2010) 405–437 [[arXiv:1002.0329](#)].
- [6] M. Fabbrichesi, E. Gabrielli, and G. Lanfranchi, “The Dark Photon.” [arXiv:2005.01515](#).
- [7] B. Holdom, “Two  $U(1)$ ’s and Epsilon Charge Shifts,” *Phys. Lett. B* **166** (1986) 196–198.
- [8] R. Foot and X.-G. He, “Comment on Z Z-prime mixing in extended gauge theories,” *Phys. Lett. B* **267** (1991) 509–512.
- [9] B. Kors and P. Nath, “Aspects of the Stueckelberg extension,” *JHEP* **07** (2005) 069 [[hep-ph/0503208](#)].
- [10] D. Feldman, Z. Liu, and P. Nath, “Probing a very narrow Z-prime boson with CDF and D0 data,” *Phys. Rev. Lett.* **97** (2006) 021801 [[hep-ph/0603039](#)].
- [11] D. Feldman, Z. Liu, and P. Nath, “The Stueckelberg Z Prime at the LHC: Discovery Potential, Signature Spaces and Model Discrimination,” *JHEP* **11** (2006) 007 [[hep-ph/0606294](#)].
- [12] D. Feldman, Z. Liu, and P. Nath, “The Stueckelberg Z-prime Extension with Kinetic Mixing and Milli-Charged Dark Matter From the Hidden Sector,” *Phys. Rev. D* **75** (2007) 115001 [[hep-ph/0702123](#)].
- [13] M. Du, Z. Liu, and V. Q. Tran, “Enhanced Long-Lived Dark Photon Signals at the LHC,” *JHEP* **05** (2020) 055 [[arXiv:1912.00422](#)].
- [14] D. Banerjee *et al.*, “Dark matter search in missing energy events with NA64,” *Phys. Rev. Lett.* **123** (2019) 121801 [[arXiv:1906.00176](#)].
- [15] Y. M. Andreev *et al.*, “Search for Light Dark Matter with NA64 at CERN.” [arXiv:2307.02404](#).
- [16] BaBar Collaboration, “Search for Invisible Decays of a Dark Photon Produced in  $e^+e^-$  Collisions at BaBar,” *Phys. Rev. Lett.* **119** (2017) 131804 [[arXiv:1702.03327](#)].
- [17] J. Alvey, M. Campos, M. Fairbairn, and T. You, “Detecting Light Dark Matter via Inelastic Cosmic Ray Collisions,” *Phys. Rev. Lett.* **123** (2019) 261802 [[arXiv:1905.05776](#)].
- [18] R. Plestid, *et al.*, “New Constraints on Millicharged Particles from Cosmic-ray Production,” *Phys. Rev. D* **102** (2020) 115032 [[arXiv:2002.11732](#)].
- [19] L. Su, W. Wang, L. Wu, J. M. Yang, and B. Zhu, “Atmospheric Dark Matter and Xenon1T Excess,” *Phys. Rev. D* **102** (2020) 115028 [[arXiv:2006.11837](#)].
- [20] M. Kachelriess and J. Tjemsland, “Meson production in air showers and the search for light exotic particles,” *Astropart. Phys.* **132** (2021) 102622 [[arXiv:2104.06811](#)].
- [21] C. A. Argüelles Delgado, K. J. Kelly, and V. Muñoz Alborno, “Millicharged particles from the heavens: single- and multiple-scattering signatures,” *JHEP* **11** (2021) 099 [[arXiv:2104.13924](#)].
- [22] M. Du, R. Fang, and Z. Liu, “Millicharged particles from proton bremsstrahlung in the atmosphere.” [arXiv:2211.11469](#).
- [23] P. Gondolo, G. Ingelman, and M. Thunman, “Charm production and high-energy atmospheric muon and neutrino fluxes,” *Astropart. Phys.* **5** (1996) 309–332 [[hep-ph/9505417](#)].
- [24] T. Pierog, I. Karpenko, J. M. Katzy, E. Yatsenko, and K. Werner, “EPOS LHC: Test of collective hadronization with data measured at the CERN Large Hadron Collider,” *Phys. Rev. C* **92** (2015) 034906 [[arXiv:1306.0121](#)].
- [25] R. Ulrich, T. Pierog, and C. Baus, “Cosmic Ray Monte Carlo Package, CRMC,” 2021. [doi:10.5281/zenodo.4558706](#).
- [26] J. Picone, A. Hedin, D. P. Drob, and A. Aikin, “NRLMSISE-00 empirical model of the atmosphere: Statistical comparisons and scientific issues,” *Journal of Geophysical Research: Space Physics* **107** (2002) SIA–15.
- [27] Particle Data Group Collaboration, “Review of Particle Physics,” *Phys. Rev. D* **98** (2018) 030001.
- [28] Particle Data Group Collaboration, “Review of Particle Physics,” *PTEP* **2022** (2022) 083C01.
- [29] T. K. Gaisser, R. Engel, and E. Resconi, *Cosmic Rays and Particle Physics: 2nd Edition*. Cambridge University Press, 2016.
- [30] J. H. Koehne, *et al.*, “PROPOSAL: A tool for propagation of charged leptons,” *Comput. Phys. Commun.* **184** (2013) 2070–2090.
- [31] V. A. Ilyin, V. V. Korenkov, and D. Perret-Gallix, eds., “The Super-Kamiokande detector,” *Nucl. Instrum. Meth. A* **501** (2003) 418–462.
- [32] Super-Kamiokande Collaboration, “Supernova Relic Neutrino Search at Super-Kamiokande,” *Phys. Rev. D* **85** (2012) 052007 [[arXiv:1111.5031](#)].
- [33] Super-Kamiokande Collaboration, “Diffuse supernova neutrino background search at Super-Kamiokande,” *Phys. Rev. D* **104** (2021) 122002 [[arXiv:2109.11174](#)].
- [34] M. Taani, *Non-Standard Neutrino Interaction Analysis with Atmospheric Neutrino Data in Super-Kamiokande I-IV and the Design of the Hyper-Kamiokande Outer Detector*. PhD thesis, Nagoya University/The University of Edinburgh, Edinburgh U., 2020.
- [35] C. A. Argüelles, *et al.*, “Dark matter annihilation to neutrinos,” *Rev. Mod. Phys.* **93** (2021) 035007 [[arXiv:1912.09486](#)].
- [36] A. A. Prinz *et al.*, “Search for millicharged particles at SLAC,” *Phys. Rev. Lett.* **81** (1998) 1175–1178 [[hep-ex/9804008](#)].
- [37] G. Magill, R. Plestid, M. Pospelov, and Y.-D. Tsai, “Millicharged particles in neutrino experiments,” *Phys. Rev. Lett.* **122** (2019) 071801 [[arXiv:1806.03310](#)].
- [38] G. Marocco and S. Sarkar, “Blast from the past: Constraints on the dark sector from the BEBC WA66 beam dump experiment,” *SciPost Phys.* **10** (2021) 043 [[arXiv:2011.08153](#)].

- [39] **SENSEI** Collaboration, “SENSEI: Search for Millicharged Particles produced in the NuMI Beam.” [arXiv:2305.04964](#).
- [40] **AMS** Collaboration, “Precision Measurement of the Proton Flux in Primary Cosmic Rays from Rigidity 1 GV to 1.8 TV with the Alpha Magnetic Spectrometer on the International Space Station,” *Phys. Rev. Lett.* **114** (2015) 171103.
- [41] P. deNiverville, C.-Y. Chen, M. Pospelov, and A. Ritz, “Light dark matter in neutrino beams: production modelling and scattering signatures at MiniBooNE, T2K and SHiP,” *Phys. Rev. D* **95** (2017) 035006 [[arXiv:1609.01770](#)].
- [42] J. L. Feng, I. Galon, F. Kling, and S. Trojanowski, “ForwArD Search Experiment at the LHC,” *Phys. Rev. D* **97** (2018) 035001 [[arXiv:1708.09389](#)].
- [43] S. Foroughi-Abari and A. Ritz, “Dark sector production via proton bremsstrahlung,” *Phys. Rev. D* **105** (2022) 095045 [[arXiv:2108.05900](#)].
- [44] M. Du, R. Fang, Z. Liu, and V. Q. Tran, “Enhanced long-lived dark photon signals at lifetime frontier detectors,” *Phys. Rev. D* **105** (2022) 055012 [[arXiv:2111.15503](#)].
- [45] A. Faessler, M. I. Krivoruchenko, and B. V. Martemyanov, “Once more on electromagnetic form factors of nucleons in extended vector meson dominance model,” *Phys. Rev. C* **82** (2010) 038201 [[arXiv:0910.5589](#)].